

Hyperon-Nucleon Interaction from Lattice QCD at (m_π, m_K) \approx (146, 525) MeV

Hidekatsu Nemura^{1,2,a)}

for HAL QCD Collaboration

¹Research Center for Nuclear Physics, Osaka University, Osaka, 567-0047, Japan

²Theoretical Research Division, Nishina Center, RIKEN, Saitama, 351-0198, Japan

^{a)}Corresponding author: hidekatsu.nemura@rcnp.osaka-u.ac.jp

Abstract. Comprehensive study of generalized baryon-baryon (BB) interaction including strangeness is one of the important subject of nuclear physics. In order to obtain a complete set of isospin-base baryon interactions, we perform a large scale lattice QCD calculation with almost physical quark masses corresponding to (m_π, m_K) \approx (146, 525) MeV and large volume (La)⁴ = (96a)⁴ \approx (8.1 fm)⁴. A large number of Nambu-Bethe-Salpeter (NBS) correlation functions from nucleon-nucleon (NN) to $\Xi\Xi$ are calculated simultaneously. In this contribution, we focus on the strangeness $S = -1$ channels of the hyperon interactions by means of HAL QCD method. Three potentials ((i) the 1S_0 central, (ii) the $^3S_1 - ^3D_1$ central, and (iii) $^3S_1 - ^3D_1$ tensor potentials) are presented for four isospin components; (1) the $\Sigma N - \Sigma N$ (the isospin $I = 3/2$) diagonal, (2) the $\Lambda N - \Lambda N$ diagonal, (3) the $\Lambda N \rightarrow \Sigma N$ transition, and (4) the $\Sigma N - \Sigma N$ ($I = 1/2$) diagonal. Scattering phase shifts for ΣN ($I = 3/2$) system are presented.

Introduction

Elucidation of generalized nuclear forces including strangeness based on the fundamental perspectives (i.e, based on degrees of freedom in terms of quarks and gluons) is one of the most important tasks of contemporary nuclear physics. For the normal nuclear interaction without strangeness, high precision experimental data are available; the interaction is described by a phenomenological approach that can reproduce the phase shifts and the deuteron properties with high accuracy. In addition, by combining a phenomenological three-nucleon force the energy levels of light nuclei can also be reproduced. On the other hand, for the hyperon-nucleon (YN) and hyperon-hyperon (YY) interactions, precise information such as phase shift analysis is limited because the scattering experiment of YN or YY system is difficult due to the hyperon short life-time. Thus far, based on the accumulation of accurate measurement of energy levels of various light hypernuclei [1] together with theoretical many-body studies [2, 3] in addition to the (limited) scattering observables, a study toward comprehensive understanding the strange nuclear forces has been made. However, our knowledge of the YN and YY interactions is still away from the level of our knowledge of the NN interaction. For the ΣN interaction, only a four-body Σ -hypernucleus ($^4_\Sigma\text{He}$) has been observed and a repulsive Σ -nucleus interaction is inferred from the recent experimental study [4]. Such quantitative understanding is useful to study properties of high dense nuclear matters such as inside neutron stars, where recent observations of massive neutron stars heavier than $2M_\odot$ might raise a puzzle for the equation of state (EOS). Furthermore, keenly understanding of general nuclear forces would be important due to the recent observation of a binary neutron star merger [5, 6].

During the last decade a new lattice QCD approach to study hadron-hadron interactions has been proposed [7, 8] and developed to enhance the accuracy [9]. In this approach, we first measure the Nambu-Bethe-Salpeter (NBS) wave function by means of the lattice QCD approach and then the interhadron potential is obtained. The scattering observables (e.g., phase shifts) and the binding energies are calculated by utilizing the potential. Thus far many studies have been performed by HAL QCD Collaboration for the various baryonic interactions [10, 11, 12, 13, 14, 15, 16, 17, 18, 19, 20, 21]. This approach is now called HAL QCD method.

In recent years, 2+1 flavor lattice QCD calculations have been extensively performed. Flavor symmetry breaking is a major concern in the study of BB interactions. Therefore this is an opportune time to study the BB potentials by using 2 + 1 flavor lattice QCD. It is advantageous to calculate a large number of NBS wave functions of various

BB channels simultaneously in a single lattice QCD calculation. In these circumstances we consider the following 52 four-point correlation functions in order to study the complete set of BB interactions in the isospin symmetric limit [22, 23]. (For the moment, we assume that the electromagnetic interaction is not taken into account in the present lattice calculation.)

$$\langle p n \overline{p n} \rangle, \quad (1)$$

$$\begin{aligned} &\langle p \Lambda \overline{p \Lambda} \rangle, \quad \langle p \Lambda \overline{\Sigma^+ n} \rangle, \quad \langle p \Lambda \overline{\Sigma^0 p} \rangle, \\ &\langle \Sigma^+ n \overline{p \Lambda} \rangle, \quad \langle \Sigma^+ n \overline{\Sigma^+ n} \rangle, \quad \langle \Sigma^+ n \overline{\Sigma^0 p} \rangle, \\ &\langle \Sigma^0 p \overline{p \Lambda} \rangle, \quad \langle \Sigma^0 p \overline{\Sigma^+ n} \rangle, \quad \langle \Sigma^0 p \overline{\Sigma^0 p} \rangle, \end{aligned} \quad (2)$$

$$\begin{aligned} &\langle \Lambda \Lambda \overline{\Lambda \Lambda} \rangle, \quad \langle \Lambda \Lambda \overline{p \Xi^-} \rangle, \quad \langle \Lambda \Lambda \overline{n \Xi^0} \rangle, \quad \langle \Lambda \Lambda \overline{\Sigma^+ \Sigma^-} \rangle, \quad \langle \Lambda \Lambda \overline{\Sigma^0 \Sigma^0} \rangle, \\ &\langle p \Xi^- \overline{\Lambda \Lambda} \rangle, \quad \langle p \Xi^- \overline{p \Xi^-} \rangle, \quad \langle p \Xi^- \overline{n \Xi^0} \rangle, \quad \langle p \Xi^- \overline{\Sigma^+ \Sigma^-} \rangle, \quad \langle p \Xi^- \overline{\Sigma^0 \Sigma^0} \rangle, \quad \langle p \Xi^- \overline{\Sigma^0 \Lambda} \rangle, \\ &\langle n \Xi^0 \overline{\Lambda \Lambda} \rangle, \quad \langle n \Xi^0 \overline{p \Xi^-} \rangle, \quad \langle n \Xi^0 \overline{n \Xi^0} \rangle, \quad \langle n \Xi^0 \overline{\Sigma^+ \Sigma^-} \rangle, \quad \langle n \Xi^0 \overline{\Sigma^0 \Sigma^0} \rangle, \quad \langle n \Xi^0 \overline{\Sigma^0 \Lambda} \rangle, \\ &\langle \Sigma^+ \Sigma^- \overline{\Lambda \Lambda} \rangle, \quad \langle \Sigma^+ \Sigma^- \overline{p \Xi^-} \rangle, \quad \langle \Sigma^+ \Sigma^- \overline{n \Xi^0} \rangle, \quad \langle \Sigma^+ \Sigma^- \overline{\Sigma^+ \Sigma^-} \rangle, \quad \langle \Sigma^+ \Sigma^- \overline{\Sigma^0 \Sigma^0} \rangle, \quad \langle \Sigma^+ \Sigma^- \overline{\Sigma^0 \Lambda} \rangle, \\ &\langle \Sigma^0 \Sigma^0 \overline{\Lambda \Lambda} \rangle, \quad \langle \Sigma^0 \Sigma^0 \overline{p \Xi^-} \rangle, \quad \langle \Sigma^0 \Sigma^0 \overline{n \Xi^0} \rangle, \quad \langle \Sigma^0 \Sigma^0 \overline{\Sigma^+ \Sigma^-} \rangle, \quad \langle \Sigma^0 \Sigma^0 \overline{\Sigma^0 \Sigma^0} \rangle, \\ &\quad \langle \Sigma^0 \Lambda \overline{p \Xi^-} \rangle, \quad \langle \Sigma^0 \Lambda \overline{n \Xi^0} \rangle, \quad \langle \Sigma^0 \Lambda \overline{\Sigma^+ \Sigma^-} \rangle, \quad \langle \Sigma^0 \Lambda \overline{\Sigma^0 \Lambda} \rangle, \end{aligned} \quad (3)$$

$$\begin{aligned} &\langle \Xi^- \Lambda \overline{\Xi^- \Lambda} \rangle, \quad \langle \Xi^- \Lambda \overline{\Sigma^- \Xi^0} \rangle, \quad \langle \Xi^- \Lambda \overline{\Sigma^0 \Xi^-} \rangle, \\ &\langle \Sigma^- \Xi^0 \overline{\Xi^- \Lambda} \rangle, \quad \langle \Sigma^- \Xi^0 \overline{\Sigma^- \Xi^0} \rangle, \quad \langle \Sigma^- \Xi^0 \overline{\Sigma^0 \Xi^-} \rangle, \\ &\langle \Sigma^0 \Xi^- \overline{\Xi^- \Lambda} \rangle, \quad \langle \Sigma^0 \Xi^- \overline{\Sigma^- \Xi^0} \rangle, \quad \langle \Sigma^0 \Xi^- \overline{\Sigma^0 \Xi^-} \rangle, \end{aligned} \quad (4)$$

$$\langle \Xi^- \Xi^0 \overline{\Xi^- \Xi^0} \rangle. \quad (5)$$

A large scale lattice QCD calculation [24] is now in progress [25, 26, 27, 28] to study the baryon interactions from NN to $\Xi\Xi$ by measuring a large number of NBS wave functions from 2 + 1 flavor lattice QCD by employing the almost physical quark masses corresponding to $(m_\pi, m_K) \approx (146, 525)$ MeV. See also Ref. [21] for a study of the $\Omega\Omega$ interaction.

The purpose of this report is to present our recent results of the $\Lambda N - \Sigma N$ systems (both isospin values, $I = 1/2$ and $3/2$) using full QCD gauge configurations. A very preliminary study had been reported at HYP2015 with small statistics of $\Lambda N - \Lambda N$ single channel data [29]. This report shows the latest results of the study, based on recent works reported in Refs. [22, 23]; the YN interactions in the strangeness $S = -1$ sector (i.e. $\Lambda N - \Lambda N$, $\Lambda N - \Sigma N$, and $\Sigma N - \Sigma N$ (both $I = 1/2$ and $3/2$)) are studied at almost physical quark masses corresponding to $(m_\pi, m_K) \approx (146, 525)$ MeV and large volume $(La)^4 = (96a)^4 \approx (8.1 \text{ fm})^4$ with the lattice spacing $a \approx 0.085 \text{ fm}$.

Outline of the HAL QCD method

In order to study the baryon-baryon interactions, we first define the equal time NBS wave function in particle channel $\lambda = \{B_1, B_2\}$ with Euclidean time t [7, 8]

$$\phi_{\lambda E}(\vec{r}) e^{-Et} = \sum_{\vec{X}} \left\langle 0 \left| B_{1,\alpha}(\vec{X} + \vec{r}, t) B_{2,\beta}(\vec{X}, t) \right| B = 2, E, S, I \right\rangle, \quad (6)$$

where $B_{1,\alpha}(x)$ ($B_{2,\beta}(x)$) denotes the local interpolating field of baryon B_1 (B_2) with mass m_{B_1} (m_{B_2}), and $E = \sqrt{k_\lambda^2 + m_{B_1}^2} + \sqrt{k_\lambda^2 + m_{B_2}^2}$ is the total energy in the center of mass system of a baryon number $B = 2$, strangeness S , and isospin I state. For $B_{1,\alpha}(x)$ and $B_{2,\beta}(x)$, we employ the local interpolating field of octet baryons in terms of up ($u_{a\alpha}(x)$), down ($d_{a\alpha}(x)$), and strange ($s_{a\alpha}(x)$) quark field operators given by

$$p_\alpha = \varepsilon_{abc} (u_a C \gamma_5 d_b) u_{c\alpha}, \quad n_\alpha = -\varepsilon_{abc} (u_a C \gamma_5 d_b) d_{c\alpha}, \quad (7)$$

$$\Sigma_\alpha^+ = -\varepsilon_{abc} (u_a C \gamma_5 s_b) u_{c\alpha}, \quad \Sigma_\alpha^- = -\varepsilon_{abc} (d_a C \gamma_5 s_b) d_{c\alpha}, \quad \Sigma_\alpha^0 = \frac{1}{\sqrt{2}} (X_{u\alpha} - X_{d\alpha}), \quad (8)$$

$$\Xi_\alpha^- = -\varepsilon_{abc} (d_a C \gamma_5 s_b) s_{c\alpha}, \quad \Xi_\alpha^0 = \varepsilon_{abc} (u_a C \gamma_5 s_b) s_{c\alpha}, \quad (9)$$

$$\Lambda_\alpha = \frac{1}{\sqrt{6}} (X_{u\alpha} + X_{d\alpha} - 2X_{s\alpha}), \quad (10)$$

where

$$X_{u\alpha} = \varepsilon_{abc} (d_a C \gamma_5 s_b) u_{c\alpha}, \quad X_{d\alpha} = \varepsilon_{abc} (s_a C \gamma_5 u_b) d_{c\alpha}, \quad X_{s\alpha} = \varepsilon_{abc} (u_a C \gamma_5 d_b) s_{c\alpha}. \quad (11)$$

The greek letters (α) represent Dirac spinor and the roman letters (a, b, c) are the indices for the color. For simplicity, we have suppressed the explicit spinor indices in parenthesis and spatial coordinates in Equations (7)-(11) and the renormalization factors in Eq. (6). Based on a set of the NBS wave functions, we define a non-local potential

$$\left(\frac{\nabla^2}{2\mu_\lambda} + \frac{k_\lambda^2}{2\mu_\lambda} \right) \delta_{\lambda\lambda'} \phi_{\lambda E}(\vec{r}) = \int d^3 r' U_{\lambda\lambda'}(\vec{r}, \vec{r}') \phi_{\lambda' E}(\vec{r}') \quad (12)$$

with the reduced mass $\mu_\lambda = m_{B_1} m_{B_2} / (m_{B_1} + m_{B_2})$.

In lattice QCD calculations, we compute the four-point correlation function defined by [9]

$$F_{\alpha\beta, JM}^{(B_1 B_2 \overline{B_3 B_4})}(\vec{r}, t - t_0) = \sum_{\vec{X}} \left\langle 0 \left| B_{1,\alpha}(\vec{X} + \vec{r}, t) B_{2,\beta}(\vec{X}, t) \overline{\mathcal{J}_{B_3 B_4}^{(JM)}(t_0)} \right| 0 \right\rangle, \quad (13)$$

where $\overline{\mathcal{J}_{B_3 B_4}^{(JM)}(t_0)} = \sum_{\alpha'\beta'} P_{\alpha'\beta'}^{(JM)} \overline{B_{3,\alpha'}(t_0) B_{4,\beta'}(t_0)}$ is a source operator that creates $B_3 B_4$ states with the total angular momentum J, M . The normalized four-point function can be expressed as

$$\begin{aligned} R_{\alpha\beta, JM}^{(B_1 B_2 \overline{B_3 B_4})}(\vec{r}, t - t_0) &= e^{(m_{B_1} + m_{B_2})(t - t_0)} F_{\alpha\beta, JM}^{(B_1 B_2 \overline{B_3 B_4})}(\vec{r}, t - t_0) \\ &= \sum_n A_n \sum_{\vec{X}} \left\langle 0 \left| B_{1,\alpha}(\vec{X} + \vec{r}, 0) B_{2,\beta}(\vec{X}, 0) \right| E_n \right\rangle e^{-(E_n - m_{B_1} - m_{B_2})(t - t_0)} + O(e^{-(E_{\text{th}} - m_{B_1} - m_{B_2})(t - t_0)}), \end{aligned} \quad (14)$$

where E_n ($|E_n\rangle$) is the eigen-energy (eigen-state) of the six-quark system and $A_n = \sum_{\alpha'\beta'} P_{\alpha'\beta'}^{(JM)} \langle E_n | \overline{B_{4,\beta'}} \overline{B_{3,\alpha'}} | 0 \rangle$. Hereafter, the spin and angular momentum subscripts are suppressed for F and R for simplicity. At moderately large $t - t_0$ where the inelastic contribution above the pion production $O(e^{-(E_{\text{th}} - m_{B_1} - m_{B_2})(t - t_0)}) = O(e^{-m_\pi(t - t_0)})$ becomes negligible, we can construct the non-local potential U through $\left(\frac{\nabla^2}{2\mu_\lambda} + \frac{k_\lambda^2}{2\mu_\lambda} \right) \delta_{\lambda\lambda'} F_{\lambda'}(\vec{r}) = \int d^3 r' U_{\lambda\lambda'}(\vec{r}, \vec{r}') F_{\lambda'}(\vec{r}')$. In lattice QCD calculations in a finite box, it is practical to use the velocity (derivative) expansion, $U_{\lambda\lambda'}(\vec{r}, \vec{r}') = V_{\lambda\lambda'}(\vec{r}, \vec{\nabla}_r) \delta^3(\vec{r} - \vec{r}')$. In the lowest few orders we have

$$V(\vec{r}, \vec{\nabla}_r) = V^{(0)}(r) + V^{(\sigma)}(r) \vec{\sigma}_1 \cdot \vec{\sigma}_2 + V^{(T)}(r) S_{12} + V^{(LS)}(r) \vec{L} \cdot (\vec{\sigma}_1 \pm \vec{\sigma}_2) + O(\nabla^2), \quad (15)$$

where $r = |\vec{r}|$, $\vec{\sigma}_i$ are the Pauli matrices acting on the spin space of the i -th baryon, $S_{12} = 3(\vec{r} \cdot \vec{\sigma}_1)(\vec{r} \cdot \vec{\sigma}_2)/r^2 - \vec{\sigma}_1 \cdot \vec{\sigma}_2$ is the tensor operator, and $\vec{L} = \vec{r} \times (-i\vec{\nabla})$ is the angular momentum operator. The first three-terms constitute the leading order (LO) potential while the fourth term corresponds to the next-to-leading order (NLO) potential. By taking the non-relativistic approximation, $E_n - m_{B_1} - m_{B_2} \simeq \frac{k_{\lambda n}^2}{2\mu_\lambda} + O(k_{\lambda n}^4)$, and neglecting the V_{NLO} and the higher order terms, we obtain

$$\left(\frac{\nabla^2}{2\mu_\lambda} - \frac{\partial}{\partial t} \right) R_{\lambda\varepsilon}(\vec{r}, t) \simeq V_{\lambda\lambda'}^{(\text{LO})}(\vec{r}) \theta_{\lambda\lambda'} R_{\lambda'\varepsilon}(\vec{r}, t), \quad \text{with} \quad \theta_{\lambda\lambda'} = e^{(m_{B_1} + m_{B_2} - m_{B_1'} - m_{B_2'})(t - t_0)}. \quad (16)$$

Note that we have introduced a matrix form $R_{\lambda'\varepsilon} = \{R_{\lambda'\varepsilon_0}, R_{\lambda'\varepsilon_1}\}$ with linearly independent NBS wave functions $R_{\lambda'\varepsilon_0}$ and $R_{\lambda'\varepsilon_1}$. For the spin singlet state, we extract the central potential as

$$V_{\lambda\lambda'}^{(\text{Central})}(r; J = 0) = (\theta_{\lambda\lambda'})^{-1} (R^{-1})_{\varepsilon'\lambda'} \left(\frac{\nabla^2}{2\mu_\lambda} - \frac{\partial}{\partial t} \right) R_{\lambda\varepsilon'}. \quad (17)$$

For the spin triplet state, the wave function is decomposed into the S - and D -wave components as

$$R(\vec{r}; {}^3S_1) = \mathcal{P}R(\vec{r}; J = 1) \equiv \frac{1}{24} \sum_{\mathcal{R} \in O} \mathcal{R}R(\vec{r}; J = 1), \quad (18)$$

$$R(\vec{r}; {}^3D_1) = \mathcal{Q}R(\vec{r}; J = 1) \equiv (1 - \mathcal{P})R(\vec{r}; J = 1). \quad (19)$$

Therefore, the Schrödinger equation with the LO potentials for the spin triplet state becomes

$$\left\{ \begin{array}{c} \mathcal{P} \\ \mathcal{Q} \end{array} \right\} \times \left\{ V_{\lambda\lambda'}^{(0)}(r) + V_{\lambda\lambda'}^{(\sigma)}(r) + V_{\lambda\lambda'}^{(T)}(r) S_{12} \right\} \theta_{\lambda\lambda'} R_{\lambda'\varepsilon}(\vec{r}, t - t_0) = \left\{ \begin{array}{c} \mathcal{P} \\ \mathcal{Q} \end{array} \right\} \times \left\{ \frac{\nabla^2}{2\mu_\lambda} - \frac{\partial}{\partial t} \right\} R_{\lambda\varepsilon}(\vec{r}, t - t_0), \quad (20)$$

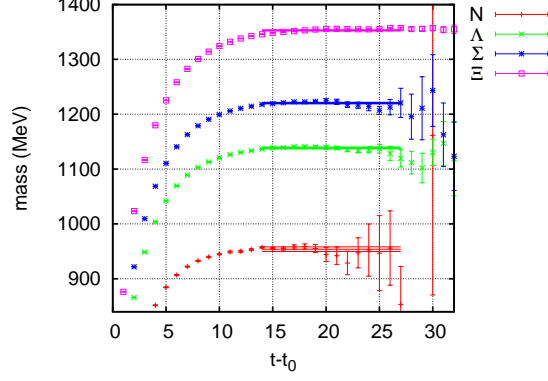


FIGURE 1. The effective mass of single baryon's correlation functions with utilizing wall sources.

from which the central and tensor potentials, $V_{\lambda\lambda'}^{(Central)}(r; J = 0) = (V^{(0)}(r) - 3V^{(\sigma)}(r))_{\lambda\lambda'}$ for $J = 0$, $V_{\lambda\lambda'}^{(Central)}(r; J = 1) = (V^{(0)}(r) + V^{(\sigma)}(r))_{\lambda\lambda'}$, and $V_{\lambda\lambda'}^{(Tensor)}(r)$ for $J = 1$, can be determined¹.

Lattice setup

2 + 1 flavor gauge configurations are generated on a 96^4 lattice by employing the RG improved (Iwasaki) gauge action at $\beta = 1.82$ with the nonperturbatively $O(a)$ improved Wilson quark (clover) action at $(\kappa_{ud}, \kappa_s) = (0.126117, 0.124790)$ with $c_{sw} = 1.11$ and the 6-APE stout smeared links with the smearing parameter $\rho = 0.1$. The lattice QCD's measurement is performed at almost the physical quark masses; see Ref. [24] for details of the generation of the gauge configuration which show that light meson masses are $(m_\pi, m_K) \approx (146, 525)$ MeV. The physical volume is $(aL)^4 \approx (8.1\text{fm})^4$ with the lattice spacing $a \approx 0.085\text{fm}$. Wall quark source is employed with Coulomb gauge fixing. For spacial direction the periodic boundary condition is used whereas for temporal direction the Dirichlet boundary condition (DBC) is used. The source and the DBC are separated by $|t_{DBC} - t_0| = 48$. Each gauge configuration is used four times by using the hypercubic $SO(4, \mathbb{Z})$ symmetry of 96^4 lattice. In order to further increase (double) the statistics forward and backward propagation in time are combined by using the charge conjugation and time reversal symmetries. A simultaneous calculation of a large number of baryon-baryon correlation functions including the channels from NN to $\Xi\Xi$ is proposed and a C++ program is implemented [22]. The other program based on unified contraction algorithm (UCA) [30] is implemented after the above work and the thoroughgoing consistency check in the numerical outputs is performed between the UCA and the present algorithm [23]. In this report, 96 wall sources are used for the 414 gauge configurations at every 5 trajectories. The number of statistics has doubled from Ref. [25]. Statistical data are averaged with the bin size 46. Jackknife method is used to estimate the statistical errors.

Results

Effective masses from single baryons' correlation function

Figure 1 shows the effective masses of the single baryon's correlation function. The plateaux start from time slices around $t - t_0 \approx 14$ for the baryons N , Λ , and Σ . When calculating the normalized four-point correlation function in Eq. (14), the exponential functional form $e^{(m_{B_1} + m_{B_2})(t-t_0)}$ is replaced by the single baryon's correlation functions, $(C_{B_1}(t - t_0)C_{B_2}(t - t_0))^{-1}$. It would be beneficial to reduce the statistical noise because of the statistical correlation between the numerator and the denominator in the normalized four-point correlation function. Therefore it is favorable

¹The potential is obtained from the NBS wave function at moderately large imaginary time; it would be $t - t_0 \gg 1/m_\pi \sim 1.4$ fm. In addition, no single state saturation between the ground state and the excited states with respect to the relative motion, e.g., $t - t_0 \gg (\Delta E)^{-1} = ((2\pi)^2/(2\mu(La)^2))^{-1} \approx 8.0$ fm, is required for the HAL QCD method [9].

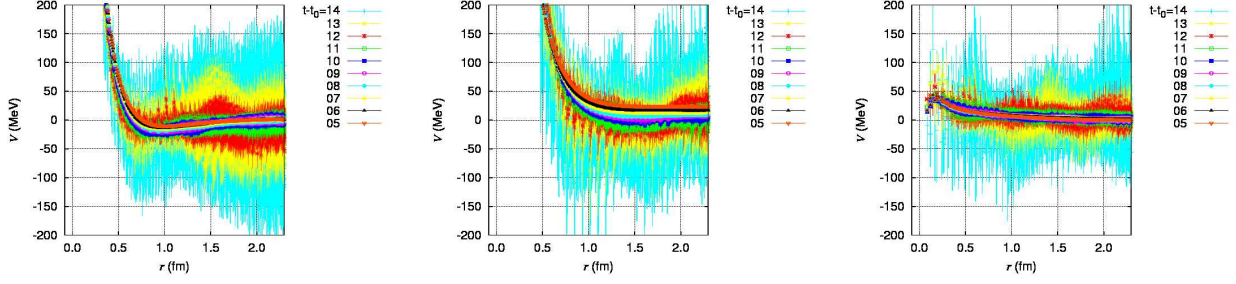


FIGURE 2. Three $\Sigma N (I = 3/2)$ potentials of (i) 1S_0 central (left), (ii) $^3S_1 - ^3D_1$ central (center), and (iii) $^3S_1 - ^3D_1$ tensor (right).

that the potentials are obtained at the time slices $t - t_0 \gtrsim 14$. In this report we present preliminary results of potentials at time slices ($t - t_0 = 5 - 14$) of our on-going work.

$\Sigma N (I = 3/2)$ system

Potentials

Fig. 2 shows three potentials of $\Sigma N (I = 3/2)$ system; (i) the central potential in the 1S_0 (left), (ii) the central potential in the $^3S_1 - ^3D_1$ (center), and (iii) the tensor potential in the $^3S_1 - ^3D_1$ (right). For the 1S_0 state there are both short ranged repulsive core and medium-to-long-distanced attractive well in the central potential. The potential is more or less similar to the NN 1S_0 because this state belongs to flavor **27** irreducible representation (*irrep*). On the other hand, in the $^3S_1 - ^3D_1$ channel a stronger repulsive core in the central potential is found. Especially the range of the repulsive core ($r \lesssim 1$ fm) is larger than the range of the repulsive core in the 1S_0 potential. This strong repulsive behavior is consistent with quark model's prediction that there is an almost Pauli forbidden state in the flavor **10** *irrep*. The tensor potential is not as strong as the NN tensor potential. The statistical fluctuation of the tensor potential becomes large at the time slices $t - t_0 \geq 11$ whereas that of the tensor potential at $t - t_0 \leq 10$ does not. These observations are consistent with the scattering phase shift calculated below.

Scattering phase shifts

In order to obtain the scattering phase shift from the lattice QCD potential obtained above we first parametrize the potential with an analytic functional form. In this report, we use following functional forms for the central and tensor potentials, respectively.

$$\begin{aligned}
 V_C(r) &= v_{C1} e^{-\kappa_{C1} r^2} + v_{C2} e^{-\kappa_{C2} r^2} + v_{C3} (1 - e^{-\alpha_C r^2})^2 \left(\frac{e^{-\beta_C r}}{r} \right)^2, \\
 V_T(r) &= v_{T1} (1 - e^{-\alpha_{T1} r^2})^2 \left(1 + \frac{3}{\beta_{T1} r} + \frac{3}{(\beta_{T1} r)^2} \right) \frac{e^{-\beta_{T1} r}}{r} + v_{T2} (1 - e^{-\alpha_{T2} r^2})^2 \left(1 + \frac{3}{\beta_{T2} r} + \frac{3}{(\beta_{T2} r)^2} \right) \frac{e^{-\beta_{T2} r}}{r}.
 \end{aligned} \tag{21}$$

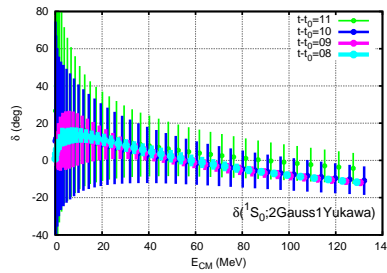


FIGURE 3. Scattering phase shift in the 1S_0 state of $\Sigma N (I = 3/2)$ system, obtained by solving the Schrödinger equation with parametrized functional form Eq. (21).

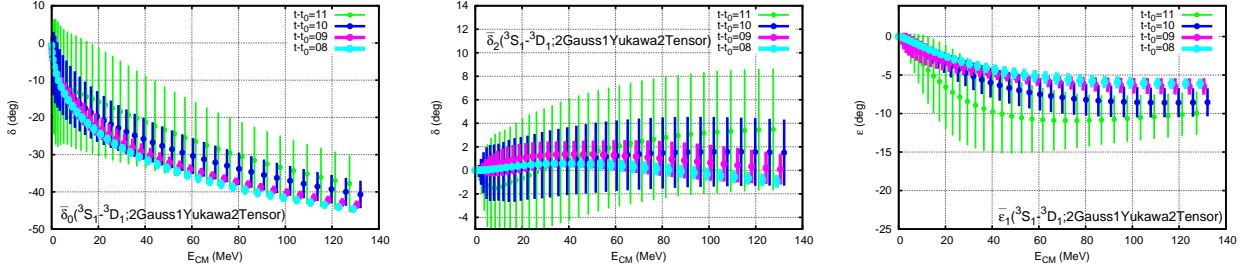


FIGURE 4. Scattering bar-phase shifts and mixing angle in the ${}^3S_1 - {}^3D_1$ states of $\Sigma N(I = 3/2)$ system, $\bar{\delta}_0$ (left), $\bar{\delta}_2$ (center), and $\bar{\epsilon}_1$ (right), obtained by solving the Schrödinger equation with parametrized functional form Eq. (21).

Figure 3 shows the scattering phase shift in 1S_0 channel of $\Sigma N(I = 3/2)$ system obtained through the above parametrized potentials. The present result shows that the interaction in the 1S_0 channel is attractive on average though the fluctuation is large especially for the time slices $t - t_0 = 10, 11$. Figure 4 shows the scattering phase shifts in ${}^3S_1 - {}^3D_1$ channels. For the ${}^3S_1 - {}^3D_1$ channels, the scattering matrix is parametrized with three real parameters bar-phase shifts and mixing angle:

$$S = \begin{pmatrix} e^{i\bar{\delta}_{J-1}} & 0 \\ 0 & e^{i\bar{\delta}_{J+1}} \end{pmatrix} \begin{pmatrix} \cos 2\bar{\epsilon}_J & i \sin 2\bar{\epsilon}_J \\ i \sin 2\bar{\epsilon}_J & \cos 2\bar{\epsilon}_J \end{pmatrix} \begin{pmatrix} e^{i\bar{\delta}_{J-1}} & 0 \\ 0 & e^{i\bar{\delta}_{J+1}} \end{pmatrix}. \quad (22)$$

The phase shift $\bar{\delta}_0$ at the time slices $t - t_0 = 9 - 11$ shows the interaction is repulsive while the phase shift $\bar{\delta}_2$ behaves around almost zero degree.

$\Lambda N - \Sigma N (I = 1/2)$ coupled-channel systems

Fig. 5 shows three $\Lambda N - \Lambda N$ diagonal potentials; (i) the central potential in the 1S_0 (left), (ii) the central potential in the ${}^3S_1 - {}^3D_1$ (center), and (iii) the tensor potential in the ${}^3S_1 - {}^3D_1$ (right). There are repulsive cores in the short distance region and medium to long range attractive well for both central potentials. In the $\Lambda N - \Lambda N$ diagonal part, the tensor potential is relatively weak. Fig. 6 shows three potentials of the $\Lambda N \rightarrow \Sigma N$ transition part; (i) the central potential in the 1S_0 (left), (ii) the central potential in the ${}^3S_1 - {}^3D_1$ (center), and (iii) the tensor potential in the ${}^3S_1 - {}^3D_1$ (right). The statistical fluctuation in the 1S_0 central potential is still large. The ${}^3S_1 - {}^3D_1$ central potential is short ranged. In the $\Lambda N \rightarrow \Sigma N$ off-diagonal part, the tensor potential shows a sizable strength although it is not as strong as the NN tensor potential. Fig. 7 shows three $\Sigma N - \Sigma N(I = 1/2)$ diagonal potentials; (i) the central potential in the 1S_0 (left), (ii) the central potential in the ${}^3S_1 - {}^3D_1$ (center), and (iii) the tensor potential in the ${}^3S_1 - {}^3D_1$ (right). Very strong repulsive core is seen in the 1S_0 central potential. The flavor $\mathbf{8}_s$ *irrep.* could influence the potential; we have $|\Sigma N\rangle = \frac{1}{\sqrt{10}}(3|\mathbf{8}_s\rangle - |\mathbf{27}\rangle)$ in the flavor SU(3) limit. The statistical fluctuations in the strongly repulsive channel seems to be large. There are short range repulsive core and medium range attractive well in the ${}^3S_1 - {}^3D_1$ central potential.

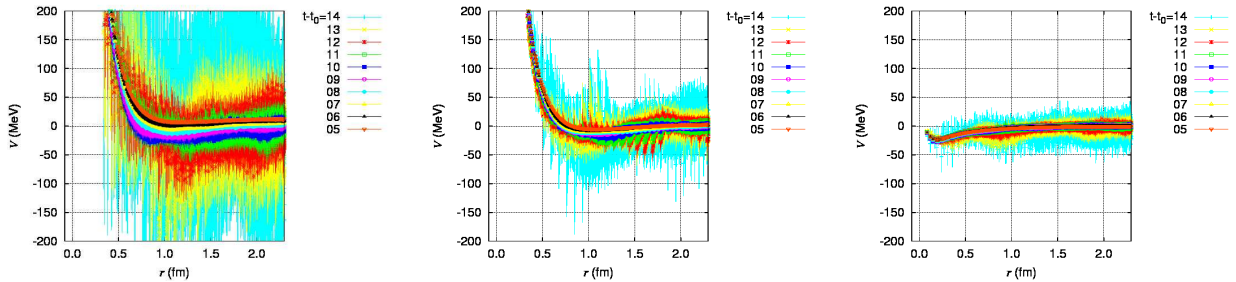


FIGURE 5. Three $\Lambda N - \Lambda N$ potentials for (i) 1S_0 central (left), (ii) ${}^3S_1 - {}^3D_1$ central (center), and (iii) ${}^3S_1 - {}^3D_1$ tensor (right).

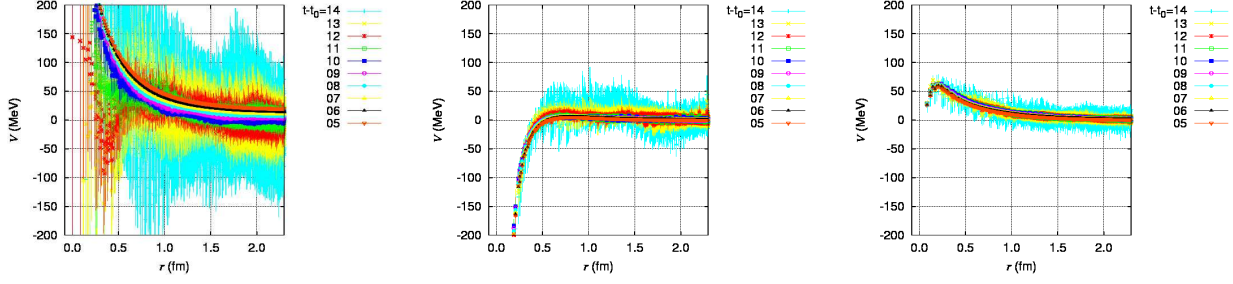


FIGURE 6. Three $\Lambda N \rightarrow \Sigma N$ potentials for (i) 1S_0 central (left), (ii) ${}^3S_1 - {}^3D_1$ central (center), and (iii) ${}^3S_1 - {}^3D_1$ tensor (right).

Summary

In this report, the study of YN interactions with $S = -1$ is presented that is based on almost physical point lattice QCD calculation. The phase shifts are calculated for the ΣN ($I = 3/2$) interaction in both the 1S_0 and ${}^3S_1 - {}^3D_1$ channels. The phase shift in the ΣN ($I = 3/2, {}^1S_0$) channel shows that the interaction is attractive on average. The phase shift $\bar{\delta}_0$ in the ${}^3S_1 - {}^3D_1$ channel shows that the ΣN ($I = 3/2, {}^3S_1$) interaction is repulsive. These results are qualitatively consistent with recent studies [31, 32, 33, 34]. In the isospin $I = 1/2$ channels, the $\Lambda N - \Sigma N$ coupled-channel potentials are presented. The potentials in the 1S_0 have still large statistical fluctuations because the number of statistics in the spin-singlet is factor 3 smaller than the number of statistics in the spin-triplet. In addition, the contribution from flavor $\mathbf{8}_s$ irrep. in the ΣN ($I = 1/2, {}^1S_0$) could break down the signal in the ΣN ($I = 1/2, {}^1S_0$) potential. Further analysis to finalize the calculations to obtain physical quantities are in progress and will be reported elsewhere.

ACKNOWLEDGMENTS

We thank all collaborators in this project, above all, members of PACS Collaboration for the gauge configuration generation. The lattice QCD calculations have been performed on the K computer at RIKEN, AICS (hp120281, hp130023, hp140209, hp150223, hp150262, hp160211, hp170230), HOKUSAI FX100 computer at RIKEN, Wako (G15023, G16030, G17002) and HA-PACS at University of Tsukuba (14a-25, 15a-33, 14a-20, 15a-30). We thank ILDG/JLDG which serves as an essential infrastructure in this study. This work is supported in part by MEXT Grant-in-Aid for Scientific Research (JP16K05340, JP25105505, JP18H05236), and SPIRE (Strategic Program for Innovative Research) Field 5 project and ‘‘Priority issue on Post-K computer’’ (Elucidation of the Fundamental Laws and Evolution of the Universe) and Joint Institute for Computational Fundamental Science (JICFuS).

REFERENCES

- [1] O. Hashimoto and H. Tamura, Prog. Part. Nucl. Phys. **57**, 564–653 (2006).
- [2] Y. Yamamoto, T. Motoba, and T. A. Rijken, Prog. Theor. Phys. Suppl. **185**, 72–105 (2010).

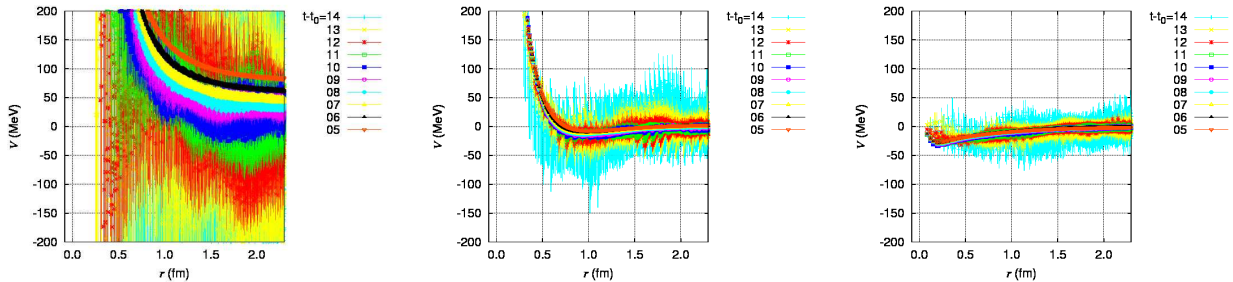


FIGURE 7. Three $\Sigma N - \Sigma N$ ($I=1/2$) potentials of (i) 1S_0 central (left), (ii) ${}^3S_1 - {}^3D_1$ central (center), and (iii) ${}^3S_1 - {}^3D_1$ tensor (right).

- [3] A. Gal, E. V. Hungerford, and D. J. Millener, *Rev. Mod. Phys.* **88**, p. 035004 (2016), arXiv:1605.00557 [nucl-th] .
- [4] H. Noumi *et al.*, *Phys. Rev. Lett.* **89**, p. 072301 (2002), [Erratum: *Phys. Rev. Lett.* 90,049902(2003)].
- [5] B. P. Abbott *et al.*, *Astrophys. J.* **848**, p. L12 (2017), arXiv:1710.05833 [astro-ph.HE] .
- [6] B. Abbott *et al.* (Virgo, LIGO Sci.), *Phys. Rev. Lett.* **119**, p. 161101 (2017), arXiv:1710.05832 [gr-qc] .
- [7] N. Ishii, S. Aoki, and T. Hatsuda, *Phys. Rev. Lett.* **99**, p. 022001 (2007), arXiv:nucl-th/0611096 [nucl-th] .
- [8] S. Aoki, T. Hatsuda, and N. Ishii, *Prog. Theor. Phys.* **123**, 89–128 (2010), arXiv:0909.5585 [hep-lat] .
- [9] N. Ishii, S. Aoki, T. Doi, T. Hatsuda, Y. Ikeda, T. Inoue, K. Murano, H. Nemura, and K. Sasaki (HAL QCD), *Phys. Lett.* **B712**, 437–441 (2012), arXiv:1203.3642 [hep-lat] .
- [10] T. Inoue *et al.* (HAL QCD Collaboration), *Nucl.Phys.* **A881**, 28–43 (2012), arXiv:1112.5926 [hep-lat] .
- [11] S. Aoki *et al.* (HAL QCD Collaboration), *Proc.Japan Acad.* **B87**, 509–517 (2011).
- [12] S. Aoki, T. Doi, T. Hatsuda, Y. Ikeda, T. Inoue, N. Ishii, K. Murano, H. Nemura, and K. Sasaki (HAL QCD), *PTEP* **2012**, p. 01A105 (2012), arXiv:1206.5088 [hep-lat] .
- [13] T. Inoue *et al.* (HAL QCD collaboration), *Phys.Rev.Lett.* **111**, p. 112503 (2013), arXiv:1307.0299 [hep-lat] .
- [14] K. Murano, N. Ishii, S. Aoki, T. Doi, T. Hatsuda, Y. Ikeda, T. Inoue, H. Nemura, and K. Sasaki (HAL QCD), *Phys. Lett.* **B735**, 19–24 (2014), arXiv:1305.2293 [hep-lat] .
- [15] T. Inoue, S. Aoki, B. Charron, T. Doi, T. Hatsuda, Y. Ikeda, N. Ishii, K. Murano, H. Nemura, and K. Sasaki (HAL QCD), *Phys. Rev.* **C91**, p. 011001 (2015), arXiv:1408.4892 [hep-lat] .
- [16] F. Etminan, H. Nemura, S. Aoki, T. Doi, T. Hatsuda, Y. Ikeda, T. Inoue, N. Ishii, K. Murano, and K. Sasaki (HAL QCD), *Proceedings, 45 Years of Nuclear Theory at Stony Brook: A Tribute to Gerald E. Brown: Stony Brook, NY, USA, November 24-26, 2013*, *Nucl. Phys.* **A928**, 89–98 (2014), arXiv:1403.7284 [hep-lat] .
- [17] K. Sasaki, S. Aoki, T. Doi, T. Hatsuda, Y. Ikeda, T. Inoue, N. Ishii, and K. Murano (HAL QCD), *PTEP* **2015**, p. 113B01 (2015), arXiv:1504.01717 [hep-lat] .
- [18] M. Yamada, K. Sasaki, S. Aoki, T. Doi, T. Hatsuda, Y. Ikeda, T. Inoue, N. Ishii, K. Murano, and H. Nemura (HAL QCD), *PTEP* **2015**, p. 071B01 (2015), arXiv:1503.03189 [hep-lat] .
- [19] T. Iritani *et al.*, *JHEP* **10**, p. 101 (2016), arXiv:1607.06371 [hep-lat] .
- [20] T. Iritani, S. Aoki, T. Doi, T. Hatsuda, Y. Ikeda, T. Inoue, N. Ishii, H. Nemura, and K. Sasaki, *Phys. Rev.* **D96**, p. 034521 (2017), arXiv:1703.07210 [hep-lat] .
- [21] S. Gongyo *et al.*, *Phys. Rev. Lett.* **120**, p. 212001 (2018), arXiv:1709.00654 [hep-lat] .
- [22] H. Nemura (HAL QCD), *Proceedings, 31st International Symposium on Lattice Field Theory (Lattice 2013): Mainz, Germany, July 29-August 3, 2013*, *PoS LATTICE2013*, p. 426 (2014).
- [23] H. Nemura, *Comput. Phys. Commun.* **207**, 91–104 (2016), arXiv:1510.00903 [hep-lat] .
- [24] K. I. Ishikawa, N. Ishizuka, Y. Kuramashi, Y. Nakamura, Y. Namekawa, Y. Taniguchi, N. Ukita, T. Yamazaki, and T. Yoshie (PACS), *Proceedings, 33rd International Symposium on Lattice Field Theory (Lattice 2015): Kobe, Japan, July 14-18, 2015*, *PoS LATTICE2015*, p. 075 (2016), arXiv:1511.09222 [hep-lat] .
- [25] H. Nemura *et al.*, *Proceedings, 35th International Symposium on Lattice Field Theory (Lattice 2017): Granada, Spain, June 18-24, 2017*, *EPJ Web Conf.* **175**, p. 05030 (2018), arXiv:1711.07003 [hep-lat] .
- [26] N. Ishii *et al.*, *Proceedings, 35th International Symposium on Lattice Field Theory (Lattice 2017): Granada, Spain, June 18-24, 2017*, *EPJ Web Conf.* **175**, p. 05013 (2018).
- [27] T. Doi *et al.*, *Proceedings, 35th International Symposium on Lattice Field Theory (Lattice 2017): Granada, Spain, June 18-24, 2017*, *EPJ Web Conf.* **175**, p. 05009 (2018), arXiv:1711.01952 [hep-lat] .
- [28] K. Sasaki, S. Aoki, T. Doi, S. Gongyo, T. Hatsuda, Y. Ikeda, T. Inoue, T. Iritani, N. Ishii, and T. Miyamoto (HAL QCD), *Proceedings, 35th International Symposium on Lattice Field Theory (Lattice 2017): Granada, Spain, June 18-24, 2017*, *EPJ Web Conf.* **175**, p. 05010 (2018).
- [29] H. Nemura *et al.*, *Proceedings, 12th International Conference on Hypernuclear and Strange Particle Physics (HYP 2015)*, *JPS Conf. Proc.* **17**, p. 052002 (2017), arXiv:1604.08346 [hep-lat] .
- [30] T. Doi and M. G. Endres, *Comput. Phys. Commun.* **184**, p. 117 (2013), arXiv:1205.0585 [hep-lat] .
- [31] Y. Fujiwara, C. Nakamoto, and Y. Suzuki, *Phys. Rev.* **C54**, 2180–2200 (1996).
- [32] I. Arisaka, K. Nakagawa, S. Shinmura, and M. Wada, *Prog. Theor. Phys.* **104**, 995–1024 (2000), [Erratum: *Prog. Theor. Phys.* 107,237(2002)].
- [33] S. R. Beane, E. Chang, S. D. Cohen, W. Detmold, H. W. Lin, T. C. Luu, K. Orginos, A. Parreno, M. J. Savage, and A. Walker-Loud, *Phys. Rev. Lett.* **109**, p. 172001 (2012), arXiv:1204.3606 [hep-lat] .
- [34] J. Haidenbauer, S. Petschauer, N. Kaiser, U. G. Meissner, A. Nogga, and W. Weise, *Nucl. Phys.* **A915**, 24–58 (2013), arXiv:1304.5339 [nucl-th] .